UNIVERSIDAD DE CONCEPCIÓN

Centro de Investigación en Ingeniería Matemática (CI^{2}MA)

Numerical simulation of forest fires by IMEX methods

Raimund Bürger, Elvis Gavilán,
Daniel Inzunza, Pep Mulet,
Luis M. Villada

PREPRINT 2020-07

SERIE DE PRE-PUBLICACIONES

Article

Numerical simulation of forest fires by IMEX methods

Raimund Bürger [1], Elvis Gavilán [2,*], Daniel Inzunza [1], Pep Mulet [3], and Luis Miguel Villada [4]

[1] CI^{2}MA and Departamento de Ingeniería Matemática, Facultad de Ciencias Físicas y Matemáticas, Universidad de Concepción, Casilla 160-C, Concepción, Chile; rburger@ing-mat.udec.cl, dinzunza@ing-mat.udec.cl

[2] Departamento de Silvicultura, Facultad de Ciencias Forestales, Universidad de Concepción, Casilla 160-C, Concepción, Chile; egavilan@udec.cl

[3] Departament de Matemàtiques, Universitat de València, Av. Vicent Andrés Estellés, E-46100 Burjassot, Spain; mulet@uv.es

[4] GIMNAP-Departamento de Matemática, Facultad de Ciencias, Universidad del Bío-Bío, Casilla 5-C, Concepción, Chile and CI^{2}MA, Universidad de Concepción, Casilla 160-C, Concepción, Chile; lvillada@ubiobio.cl

[*] Correspondence: egavilan@udec.cl

Received: date; Accepted: date; Published: date

Abstract: Numerical techniques for approximate solution of a system of reaction-diffusion-convection problem modelling the evolution of temperature and fuel density in a wildfire are introduced. These schemes combine linearly implicit-explicit Runge-Kutta (IMEX-RK) methods and Strang-type splitting technique. Numerical examples with parameters and scenarios similar to those of [Asensio, M.I.; Ferragut, L. On a wildland fire model with radiation. *Int. J. Numer. Meth. Engrg.* **2002**, *54*, 137–157] are presented. Simulations also demonstrate that the model provides a tool for defining parameters of wildland fire control strategies such as the width of firebreaks.

Keywords: Wildland fire simulation; nonlinear convection-diffusion-reaction problems; implicit-explicit method

1. Introduction

1.1. Scope

It is the purpose of this contribution to provide an efficient numerical method for the solution of a wildland fire model [2] that can be expressed as a convection-diffusion-reaction system of the type

$$\frac{\partial u}{\partial t} + \boldsymbol{w}(\boldsymbol{x},t)\cdot\nabla u = \nabla\cdot\big(K(u)\nabla u\big) + f(u,v,\boldsymbol{x}), \quad \frac{\partial v}{\partial t} = g(u,v), \tag{1.1}$$

where t is time, $\boldsymbol{x}\in\Omega$ is the spatial variable where $\Omega\subset\mathbb{R}^2$, and $u = u(\boldsymbol{x},t)$ and $v = v(\boldsymbol{x},t)$ are the sought scalar functions where u represents the non-dimensionalized temperature and v the non-dimensionalized mass fraction of solid fuel. Moreover, K is a given diffusive coefficient that depends only on u and $\boldsymbol{w}$ is an advection velocity that represents wind speed, where we assume that $\operatorname{div}\boldsymbol{w} = 0$. The functions $f(u,v,\boldsymbol{x})$ and $g(u,v)$ are the reactive part of the model. (The ingredients will be specified further below.) The dynamics of the evolution of a wildfire for an initial conditions u_0 and v_0 is described by the system (1.1) together with zero-flux boundary conditions

$$(u\boldsymbol{w} - K(u)\nabla u)\cdot\boldsymbol{n} = 0, \qquad (\boldsymbol{x},t)\in\partial\Omega\times(0,+\infty), \tag{1.2}$$

where $\boldsymbol{n}$ is the unit normal vector to $\partial\Omega$, and the initial conditions

$$u(\boldsymbol{x},0) = u_0(\boldsymbol{x}), \quad v(\boldsymbol{x},0) = v_0(\boldsymbol{x}) \qquad \boldsymbol{x}\in\Omega. \tag{1.3}$$

Explicit numerical schemes for (1.1) on a uniform Cartesian grid of meshwidth Δx and time step Δt are easy to implement but are associated with a Courant-Friedrichs-Lewy (CFL) stability condition that requires the proportionality $\Delta t \approx \Delta x^2$, which makes long-term simulations of (1.1)–(1.3) on a uniform grid unacceptably slow. A well-known remedy consists in handling the diffusive term in (1.1) by an implicit discretization. The resulting semi-implicit or implicit-explicit (IMEX) schemes (cf., e.g., [6,14]) are associated with an acceptable CFL condition $\Delta t \approx \Delta x$ but the case that K depends nonlinearly on u needs to be handled by special nonlinear solvers [14] or by solving linear problems in each time step that arise from carefully distinguishing between stiff and nontiff unknowns in the discretized version of $\nabla \cdot \big(K(u)\nabla u\big)$ [6]. These variants will be addressed as nonlinearly implicit (NI-IMEX) and linearly implicit (LI-IMEX) schemes, respectively. In this work we focus on the implementation of the linearly implicit (LI-IMEX) schemes. On the other hand, the reaction term for this model imposes a very severe restriction on the global time step Δt. As a strategy to avoid this restriction, we propose a variant of the LI-IMEX scheme consisting in a Strang-type splitting technique. This technique consists in solving the convection-diffusion system for u and coupling this result with the result of solving the ordinary differential equation (ODE) for u and v defined by the reaction terms (in which the convective and diffusive term is absent). This results in a numerical scheme that allows a less restrictive time step Δt.

From a practical point of view, we address the importance of bing able to simulate the effects of artificial firebreaks as a measure of prevention and control of forest fires. The effectiveness of a firebreak, which normally correspond to an area with no fuel availability created by cutting a lane into a forest, is strongly determined by its width, as is discussed in [22,23]. This motivates the implementation of scenarios, such as those shown here, in order to help solve the problem of determining an adequate width and thus protect a certain area from forest fire.

1.2. Related work

The literature shows many approaches to studying forest fires such as physical models, cellular automata, and artificial intelligence to name a few. A general survey on the principles of mathematical modelling of forest fires is provided by Pastor et al. [25] and more recently by Eberle et al. [17]. Most continuous-in-space approaches to model and study forest fires leads to partial differential equations (PDEs) as local forms of the balance equations that describe fuel consumption and heat transfer. A discussion of recent developments of PDE-based forest fire models, as opposed to those based on cellular automata, is included in [27]. We herein directly use the two-PDE model formulated by Asensio and Ferragut [2], which is widely accepted and has laid the foundation for various developments such as the inclusion of vegetation, moisture and endothermic pyrolisis by means of a multivalued function representing the enthalpy [18,19]. Reports of inclusion of the model by Asensio and Ferragut [2] into software packages for real scenarios include [17,26,28]. For sake of completeness, we mention that PDE-based models have also been developed for a refined description of the combustion front of a wildfire; see e.g. [3] and the references cited in that work.

Solutions to the model (1.1) may be obtained through numerical methods such as mixed finite elements, finite differences, or finite volumes. Due to the structure of the equation (1.1), a wide theory is available to implement a spatial semi-discretization of the model following a method-of-lines strategy. The resulting scheme turns out to be explicit due to the choice of ODE integrators. However, the explicit schemes applied to diffusion-reaction problems strongly restrict the passage of time due to stable conditions. Therefore, our goal is to treat diffusion-reaction implicitly and convection explicitly. To avoid the need to solve nonlinear systems that appear in the implicit treatment of nonlinear diffusion, we propose LIMEX Runge-Kutta schemes introduced in [6,7]. References to the various applications of IMEX methods for convection-diffusion-reaction problems, convection problems with stiff reaction term, hyperbolic systems with relaxation, and semi-discrete PDE solution are included in [1,6,7,14,16,24].

1.3. Outline of the paper

The remainder of the paper is organized as follows. In Section 2 the governing mathematical model is introduced. To this end, we formulate a model which is described in simplified form for the variables temperature and fuel density in terms of a system of PDEs in Section 2.2. Section 3 is devoted to the description of the numerical schemes proposed to solve the spatio-temporal model developed in Section 2.3. Values of the parameters of the model and an estimatte of the maximum temperature attainable are provided in Section 2.4. Section 3.1 introduces the notation for two numerical schemes and details the discretization of the convective flux by means of a fifth-order WENO discretization. In Section 3.2 the linearly implicit IMEX-RK method and in Section 3.3 the linearly implicit method IMEX-RK with Strang-type splitting are outlined. Section 4 is devoted to the presentation of numerical results. The examples correspond to four different scenarios. The first shows the numerical solution of the model considering an initial ignition which is in a domain where a constant fuel density is present. Results of this example, which also include a study of approximate L^1 errors, are shown in Section 4.1. In the second case we also impose an initial ignition but now with a terrain separated into two parts with different initial values for the fuel density. In the third we assume that the two regions that differ in the initial value for the fuel density are separated by a firebreak. In the fourth and last case we show the evolution of the variables in a terrain with random fuel density adding the fact that the wind undergoes a slight change in its direction. The corresponding numerical examples are presented in Sections 4.2, 4.3, and 4.4, respectively. Conclusions are collected in Section 5.

2. Mathematical model

2.1. Model development

The mathematical model follows the presentation by Asensio and Ferragut [2]. In a simplified setting, we consider the amount of solid fuel, but not its composition. The simplified chemical reaction is of the type

$$\text{fuel} + \text{oxidants} \xrightarrow{r} \text{products}.$$

The reaction-rate constant is given by the empirical Arrhenius expression

$$r = A \exp\left(-\frac{E_A}{RU}\right),$$

where R is the universal gas constant ($R = 1.987207\,\text{cal}/(\text{K mol})$), U is absolute temperature and the constant E_A denotes activation energy. A typical value is $E_A \approx 20\,\text{kcal/mol}$ [4]. The factor A may depend weakly on U (as is discussed in [2]), but is chosen to be constant here. Furthermore, let Y_f and Y_o denote the mass fraction of fuel and oxidant, respectively. If there is a sufficient amount of oxidant provided by air, that is, $Y_f \gg Y_o$, then we may assume that the fuel disappearance rate for this reaction S_f, is controlled by $Y = Y_f$, so we have

$$S_f = -A \exp\left(-\frac{E_A}{RU}\right)\rho Y,$$

where ρ is the density, and we may ignore the conservation law for the oxidant [2]. In the vicinity of a large fire source, radiation is nearly always the dominant mode of heat transfer that provides the heat of gasification necessary to liberate the fuel volatiles from their condensed phase, and which in turn react with oxygen to release further heat in addition to the gaseous and particulate products of combustion. Thermal radiation enters the set of conservation equations directly only through the divergence of the mean radiative energy flux in the energy conservation equation. Heat flux transfer by radiation through a semi-transparent substance, such as a fuel bed, is given by the Stefan-Boltzmann

law $q = -\sigma(U^4(\boldsymbol{x}+\boldsymbol{\delta}) - U^4(\boldsymbol{x}))$, where σ is the Stefan-Boltzmann constant, $\delta = \|\boldsymbol{\delta}\|$ is the length of the optical path for radiation through the substance, and U is the absolute temperature. By a linear Taylor expansion we obtain that the heat flux by radiation is given by

$$q = -4\sigma\delta U^3 \nabla U.$$

Wind tips the flame forward and causes direct flame contact with the fuel ahead of the fire as well as increased radiation from the flame to the fuel. This greatly increases the transfer of radiant and convective heat to unburned fuel ahead of the fire. The effect of slope is similar, fires spread faster upslope as the slope steepness increases, but this effect is much lesser than that of wind.

Vertical heat loss due to the effect of gravity over the different densities caused from the distinct temperatures is represented with a natural convection term within the energy conservation equation, $h(\boldsymbol{x})(U - U_\infty)$, where U_∞ is the ambient temperature and h is the natural convection coefficient. This vertical heat loss is less when there is a slope and part of the heat is transferred upslope. This corresponds to smaller values of h and to the presence of a convective term, and allows us to assume a two-dimensional model. In any case we assume that $h = h(\boldsymbol{x})$ to be able to incorporate information on the terrain. Convection of heat due to wind is modelled by a term $\rho C \boldsymbol{v}(\boldsymbol{x}, t)$, where ρ and C are the density and specific heat of the fluid, and $\boldsymbol{v}(\boldsymbol{x}, t)$ is the wind velocity vector that also represents the effect of slope. The temperature and velocity of the fluid represent averaged values in a turbulent regimen. With regard to the reactive term we have maintained the usual model of the laminar regimen. A realistic model involves evaluating a better modelling of the turbulence.

The energy released in an exothermic reaction in a laminar regimen is usually modelled by

$$Q = HS_\mathrm{f} = -HA \exp\left(-\frac{E_\mathrm{A}}{RU}\right)\rho Y,$$

where H is the heat of combustion. Previous investigators have considered different equations for each of the two phases, the endothermic or solid phase and the exothermic or gaseous phase. The change between the phases is described by the phase change function

$$s(U) := \begin{cases} 1 & \text{if } U \geq U_\mathrm{pc}, \\ 0 & \text{if } U < U_\mathrm{pc}, \end{cases}$$

where U_pc is the phase change temperature, to represent both phases with the same system of equations, taking into account that the actual disappearance of fuel and the generation of heat occur when the temperature gets past the phase change temperature.

2.2. Simplified model in final form

Combining the previous ingredients, we obtain the following model:

$$\rho C\left(\frac{\partial U}{\partial t} + \boldsymbol{w}\cdot\nabla U\right) - \nabla\cdot\left((4\sigma\delta U^3 + k)\nabla U\right) = s(U)HA\exp\left(-\frac{E_\mathrm{A}}{RU}\right)\rho Y - h(\boldsymbol{x})(U - U_\infty), \quad (2.1)$$

$$Y_t = -s(U)YA\exp\left(-\frac{E_\mathrm{A}}{RU}\right). \quad (2.2)$$

We study the model (2.1), (2.2) on a two-dimensional domain $\Omega \subset \mathbb{R}^2$ with a piecewise smooth boundary $\Gamma = \partial\Omega$ and assume that Ω is large enough so that U and Y do not change on Γ during the simulation time $(0, t_\mathrm{max})$. We may therefore impose either zero-flux or Dirichlet boundary conditions. Note that spatial heterogeneity can be represented by specifying the functions $h = h(\boldsymbol{x})$ and the initial distribution of available fuel $Y_0 = Y_0(\boldsymbol{x})$.

2.3. Dimensionless variables

The combustion model (2.1), (2.2) can be non-dimensionalized in a rational manner in order to elucidate the significant parameters. We use the Frank-Kamenetskii [20] change of variables (see [5]). We fix a reference value for the temperature and the fuel in which an equilibrium can be assumed, namely the ambient temperature $U_{\text{ref}} = U_\infty$ and the initial fuel; since Y_0 may be variable, we set

$$Y_{\text{ref}} := \frac{1}{|\Omega|}\int_\Omega Y_0(\boldsymbol{x})\,\mathrm{d}\boldsymbol{x};$$

likewise, we define

$$h_{\text{ref}} := \frac{1}{|\Omega|}\int_\Omega h(\boldsymbol{x})\,\mathrm{d}\boldsymbol{x}.$$

Furthermore we assume that t_0 and l_0 are characteristic magnitudes for temporal and spatial variables to be fixed later. The non-dimensional change is defined as follows, where we assume that $\boldsymbol{x} = (x_1, x_2)$:

$$\xi = x_1/l_0, \quad \eta = x_2/l_0, \quad \tau = t/t_0, \quad u = \frac{U - U_\infty}{\varepsilon U_\infty}, \quad v = Y/Y_{\text{ref}}, \quad \boldsymbol{w} = (t_0/l_0)\boldsymbol{v},$$

where ε is the non-dimensional inverse of the activation energy, that is $\varepsilon = RT_\infty/E_{\text{A}}$. Furthermore, we define the non-dimensional reaction heat $q_{\text{react}} = HY_{\text{ref}}/(CT_\infty)$ and the time and length scales

$$t_0 = \frac{\varepsilon}{qA}\exp(1/\varepsilon), \quad l_0 = \left(\frac{t_0 k}{\rho C}\right)^{1/2}.$$

We define the non-dimensional natural convection coefficient $\alpha = \alpha(\xi, \eta)$, the non-dimensional inverse of the conductivity coefficient κ and the non-dimensional phase change function $c(u)$ by the respective expressions

$$\alpha(\xi,\eta) = \frac{t_0 h(l_0\xi, l_0\eta)}{\rho C}, \quad \kappa = \frac{4\sigma\delta T_\infty^3}{k}, \quad c(u) = \begin{cases} 1 & \text{if } u \geq u_{\text{pc}}, \\ 0 & \text{if } u < u_{\text{pc}}, \end{cases} \quad \text{where} \quad u_{\text{pc}} = \frac{U_{\text{pc}} - U_\infty}{\varepsilon U_\infty}.$$

For simplicity, let us recover the notation t, x_1 and x_2 for non-dimensional temporal and spatial variables, $\Omega \times (0, t_{\max})$ for the non-dimensional domain, and maintain u for the non-dimensional average temperature and v for the non-dimensional mass fraction of solid fuel. Then the model can be written in the form (1.1) if we define

$$\begin{aligned} K(u) &= \kappa(1+\varepsilon u)^3 + 1, \\ f(u, v, \boldsymbol{x}) &= c(u) v \exp\left(\frac{u}{1+\varepsilon u}\right) - \alpha(\boldsymbol{x}) u, \\ g(u, v) &= -\frac{c(u)\varepsilon v}{q_{\text{react}}}\exp\left(\frac{u}{1+\varepsilon u}\right). \end{aligned} \tag{2.3}$$

2.4. Parameters used for the wildfire model

We assume an ambient temperature of $U_\infty = 303\,\text{K}$ and an activation energy $E_{\text{A}} = 20\,\text{kcal/mol} = 83.68\,\text{kJ/mol}$, which yields $\varepsilon = 0.02980905 \approx 0.03$. Furthermore, we select $A = 10^9\,\text{s}^{-1}$ [4]. Acocrding to [2], realistic values of density ρ for different kinds of wood vary from $\rho = 420\,\text{kg m}^{-3}$ (for fir) to $640\,\text{kg/m}^3$ (for yellow pine); the specific heat varies from $C = 2.4\,\text{kJ kg}^{-1}\,\text{K}^{-1}$ (for maple or oak) to $C = 2.8\,\text{kJ kg}^{-1}\,\text{K}^{-1}$ (for yellow pine), and the thermal conductivity ranges from $k = 0.059\,\text{W m}^{-1}\,\text{K}^{-1}$ (for maple or oak) to $k = 1.17\,\text{W m}^{-1}\,\text{K}^{-1}$ for sawdust. On the other hand, the values for air at atmospheric pressure and ambient temperature are $\rho = 1.1774\,\text{kg m}^{-3}$, $C = 1.0057\,\text{kJ kg}^{-1}\,\text{K}^{-1}$ and

$k = 0.024\,\mathrm{W\,m^{-1}\,K^{-1}}$. The mean magnitudes for the numerical examples in [2], and which we adopt for our numerical experiments, are

$$\rho = 100\,\mathrm{kg\,m^{-3}}, \quad C = 1\,\mathrm{kJ\,kg^{-1}\,K^{-1}}, \quad k = 1\,\mathrm{W\,m^{-1}\,K^{-1}}. \tag{2.4}$$

Asensio and Ferragut [2] argue furthermore that the heat of combustion for cellulose is $H = 15900\,\mathrm{kcal\,kg^{-1}}$, but that the presence of fuels with lower heats of combustion justifies smaller values of H. They choose H in such a way that

$$q_{\mathrm{react}} = \frac{HY_{\mathrm{ref}}}{CU_\infty} = 1.$$

If we set $Y_0 = 1$, then this corresponds to $H = 300\,\mathrm{kJ\,kg^{-1}} = 71.702\,\mathrm{kcal\,kg^{-1}}$. Utilizing the parameters (2.4), we get

$$t_0 = \frac{0.03}{10^9\,\mathrm{s^{-1}}}\exp(1/0.03) = 8986.8\,\mathrm{s}, \quad l_0 = (0.089868\,\mathrm{m^2})^{1/2} = 0.2998\,\mathrm{m}.$$

In some of the numerical examples we keep h constant and small, such that $\alpha = 10^{-3}$. The inverse of the conductivity coefficient is chosen as $\kappa = 0.1$, and we choose non-dimensional wind velocities in a different way in each example.

At the moment we do not have access to the specific value of U_{pc}. However, we may estimate the maximal temperature $u_{\max}$ that is attainable. To this end, we examine the ODE system (3.4), this means

$$\frac{\mathrm{d}u}{\mathrm{d}t} = -\frac{q_{\mathrm{react}}}{\varepsilon}\frac{\mathrm{d}v}{\mathrm{d}t}.$$

On the other hand, the second equation in (3.4) implies that $\mathrm{d}v/\mathrm{d}t \leq 0$, while $v(t) \geq 0$ if $v(0) \geq 0$. Thus we conclude that

$$u(t) = -\frac{q_{\mathrm{react}}}{\varepsilon}v(t) + \frac{q_{\mathrm{react}}}{\varepsilon}v(0) + u(0) \leq \frac{q_{\mathrm{react}}}{\varepsilon}v(0) + u(0) =: u_{\max}.$$

For instance, assume that at some point in the spatial domain we impose the initial temperature such that $u(0) = 30$, which corresponds to $U = (1 + 30\varepsilon)U_\infty = 1.9U_\infty = 570\,\mathrm{K}$, then we get $u_{\max} = (1/\varepsilon) + 30 = 63.\bar{3}$, or equivalently, a maximum temperature (in absolute value) of $U_{\max} = (1 + \varepsilon u_{\max})U_\infty = 870\,\mathrm{K}$. In light of this calculation we will choose either $u_{\mathrm{pc}} = 0$ or $0 < u_{\mathrm{pc}} \leq u(0) < u_{\max}$, where $u(0)$ is the dimensionless temperature at the point where the fire starts.

3. Numerical method

3.1. Notation and semi-discrete formulation

We take $\Omega = [0, L] \times [0, L]$ and denote by $u : \Omega \times (0, \infty) \to [0, \infty]$ and $v : \Omega \times (0, \infty) \to [0, 1]$ the solution of (1.1), where it is understood that the functions K, f and g are given by (2.3). We use a uniform Cartesian grid with nodes (x_i, y_j), $i, j = 1, \ldots, M$, with $x_i = y_i = (i - 1/2)h$ and $h = L/M$. This creates a number of M^2 grid points which we indicate by $\boldsymbol{i} = (i, j) \in \mathcal{M}$, where we define the index set $\mathcal{M} := \{1, \ldots, M\} \times \{1, \ldots, M\} \subset \mathbb{N}^2$ and denote $\boldsymbol{x_i} := (x_i, y_j)$, and utilize two-dimensional unit vectors $\boldsymbol{e}_1 = (1, 0)$ and $\boldsymbol{e}_2 = (0, 1)$ to address neighbouring grid points $\boldsymbol{x}_{\boldsymbol{i}+\boldsymbol{e}_1} = (x_{i+1}, y_j)$ and $\boldsymbol{x}_{\boldsymbol{i}+\boldsymbol{e}_2} = (x_i, y_{j+1})$. We define $\boldsymbol{u} : [0, \infty) \to \mathbb{R}^{M^2}$ as a solution computed at an instant t in the grid points

where $\boldsymbol{u}_i(t) = u(\boldsymbol{x}_i, t)$ for $\boldsymbol{i} \in \mathcal{M}$. Notation is similar for $\boldsymbol{v} : [0, \infty) \to \mathbb{R}^{M^2}$, and by simplicity we denote $K_i = K(\boldsymbol{u}_i)$ and for the reactive part we define

$$f(u, v, \boldsymbol{x}) = v\zeta(u) - \alpha(\boldsymbol{x}), \quad g(u, v) := -\frac{\varepsilon v \zeta(u)}{q_{\text{react}}} \quad \text{with} \quad \zeta(u) := c(u) \exp\left(\frac{u}{1 + \varepsilon u}\right).$$

Using this notation, we may approximate (1.1), (2.3) in semi-discrete form (that is, in discrete in space but continuous in time form) by the system of ODEs

$$\frac{\mathrm{d}\boldsymbol{u}}{\mathrm{d}t} = \mathcal{C}(\boldsymbol{u}) + \mathcal{D}(\boldsymbol{u})\boldsymbol{u} - \mathcal{A}\boldsymbol{u} + \boldsymbol{v}\zeta(\boldsymbol{u}), \quad \frac{\mathrm{d}\boldsymbol{v}}{\mathrm{d}t} = -\frac{\varepsilon}{q_{\text{react}}}\boldsymbol{v}\zeta(\boldsymbol{u}), \tag{3.1}$$

where $\mathcal{C}(\boldsymbol{u})$ and $\mathcal{D}(\boldsymbol{u})\boldsymbol{u}$ represent the spatial discretizations of the convective and diffusive terms with entries given by $\mathcal{C}(\boldsymbol{u}) = (C(\boldsymbol{u})_i)_{i \in \mathcal{M}}$, $\mathcal{D}(\boldsymbol{u})\boldsymbol{u} = ((D(\boldsymbol{u})\boldsymbol{u})_i)_{i \in \mathcal{M}}$ given by

$$\begin{aligned} C(\boldsymbol{u})_{\boldsymbol{i}} &= -\sum_{l=1}^{2} \frac{1}{\Delta x}\left(\hat{f}_{\boldsymbol{i}+\frac{1}{2}\boldsymbol{e}_l} - \hat{f}_{\boldsymbol{i}-\frac{1}{2}\boldsymbol{e}_l}\right), \\ \left(D(\boldsymbol{u})\boldsymbol{u}\right)_{\boldsymbol{i}} &= \sum_{l=1}^{2} \frac{1}{2\Delta x^2}\left((K_{\boldsymbol{i}} + K_{\boldsymbol{i}-\boldsymbol{e}_l})\boldsymbol{u}_{\boldsymbol{i}-\boldsymbol{e}_l} - (K_{\boldsymbol{i}-\boldsymbol{e}_l} + 2K_{\boldsymbol{i}} + K_{\boldsymbol{i}+\boldsymbol{e}_l})\boldsymbol{u}_{\boldsymbol{i}} + (K_{\boldsymbol{i}} + K_{\boldsymbol{i}+\boldsymbol{e}_l})\boldsymbol{u}_{\boldsymbol{i}+\boldsymbol{e}_l}\right), \end{aligned}$$

where $\hat{f}_{\boldsymbol{i}+\frac{1}{2}\boldsymbol{e}_l}$ is the fifth-order WENO spatial discretization of the convective term $\boldsymbol{w} \cdot \nabla u$ [14]. The remaining terms in (3.1) correspond to evaluations of the reactive terms that are computed in a component-wise manner, i.e., $(\mathcal{A}\boldsymbol{u})_{\boldsymbol{i}} = (\alpha(\boldsymbol{x}_{\boldsymbol{i}})\boldsymbol{u}_{\boldsymbol{i}})$ and $(\boldsymbol{v}\zeta(\boldsymbol{u}))_{\boldsymbol{i}} = (\boldsymbol{v}_{\boldsymbol{i}}\zeta(\boldsymbol{u}_{\boldsymbol{i}}))$.

The approximate solution of (3.1) can be obtained by application of Runge-Kutta ODE solvers. Strong Stability Preserving (SSP) explicit Runge-Kutta methods are a popular class of time integrators whose use leads to a stronger stability constraint on Δt, see [1,6–9,12–14,16] . An alternative to explicit RK schemes are implicit-explicit Runge-Kutta (IMEX-RK) methods (see [12–14]), for which only the diffusion term is treated implicitly. In this case the stability condition on Δt is less severe than for explicit RK schemes, but a large number of nonlinear systems are necessary to solve. To overcome the excessive numerical work for the solution of nonlinear systems, an essential gain is obtained by the approach proposed in [6,7] that is based on linearly implicit-explicit Runge-Kutta schemes. The approach for (1.1) is based on distinguishing in (3.1) between stiff and non-stiff dependence of various terms on the solution vectors $\boldsymbol{u}$ and $\boldsymbol{v}$, and in choosing the time discretization by an implicit and an explicit RK scheme for the terms involving stiff and non-stiff dependence, respectively. In the product $\mathcal{D}(\boldsymbol{u})\boldsymbol{u}$ the occurrence of the solution $\boldsymbol{u}$ within $\mathcal{D}(\boldsymbol{u})$ is considered non-stiff, while that of the factor $\boldsymbol{u}$ is considered stiff. On the other hand, in the product $\boldsymbol{v}\zeta(\boldsymbol{u})$, the term $\zeta(\boldsymbol{u})$ is considered non-stiff, while the term $\boldsymbol{v}$ is considered stiff.

3.2. Linearly implicit IMEX-RK scheme

Next, we define the following functions, which are given by the right-hand sides of (3.1) where we have replaced the argument $\boldsymbol{u}$ by $\boldsymbol{u}^*$ in all terms for which the dependence is non-stiff, and which will therefore be discretized in an explicit form:

$$\mathcal{K}^u(\boldsymbol{u}^*, \boldsymbol{u}, \boldsymbol{v}) := \mathcal{C}(\boldsymbol{u}^*) + \mathcal{D}(\boldsymbol{u}^*)\boldsymbol{u} - \mathcal{A}\boldsymbol{u} + \boldsymbol{v}\zeta(\boldsymbol{u}^*), \quad \mathcal{K}^v(\boldsymbol{u}^*, \boldsymbol{v}) := -\frac{\varepsilon}{q_{\text{react}}}\boldsymbol{v}\zeta(\boldsymbol{u}^*).$$

Then we rewrite (3.1) in the form

$$\frac{\mathrm{d}\boldsymbol{u}^*}{\mathrm{d}t} = \mathcal{K}^u(\boldsymbol{u}^*, \boldsymbol{u}, \boldsymbol{v}), \quad \frac{\mathrm{d}\boldsymbol{u}}{\mathrm{d}t} = \mathcal{K}^u(\boldsymbol{u}^*, \boldsymbol{u}, \boldsymbol{v}), \quad \frac{\mathrm{d}\boldsymbol{v}}{\mathrm{d}t} = \mathcal{K}^v(\boldsymbol{u}^*, \boldsymbol{v}). \tag{3.2}$$

Observe that the only stiff terms, which are treated implictly, are the linear terms that multiply $\mathcal{D}(\boldsymbol{u})$ and $\mathcal{A}$ in $\mathcal{K}^{\boldsymbol{u}}(\boldsymbol{u}^*, \boldsymbol{u}, \boldsymbol{v})$ and $\zeta(\boldsymbol{u})$ in $\mathcal{K}^{\boldsymbol{v}}(\boldsymbol{u}^*, \boldsymbol{v})$. Thus, we treat $\boldsymbol{u}^*$ explicitly as argument of $\mathcal{C}$, $\mathcal{D}$ and h. The pair of Butcher arrays [15] of IMEX-RK methods for the time integration of (3.2) is given by

$$\mathcal{A}_{\text{ERK}} := \begin{array}{c|c} \tilde{\boldsymbol{c}} & \tilde{\boldsymbol{A}} \\ \hline & \tilde{\boldsymbol{b}}^{\mathrm{T}} \end{array}, \qquad \mathcal{A}_{\text{DIRK}} := \begin{array}{c|c} \boldsymbol{c} & \boldsymbol{A} \\ \hline & \boldsymbol{b}^{\mathrm{T}} \end{array},$$

where $\tilde{\boldsymbol{A}} = (\tilde{a}_{ij})$ (with $\tilde{a}_{ij} = 0$ for all $j \geq i$) and $\boldsymbol{A} = (a_{ij})$ (with $a_{ij} = 0$ for all $j > i$) are the $s \times s$ matrices of the explicit (ERK) and (diagonally) implicit (DIRK) parts of the method, respectively, while $\tilde{\boldsymbol{b}} = (\tilde{b}_1, \ldots, \tilde{b}_s)^{\mathrm{T}}$, $\tilde{\boldsymbol{c}} = (\tilde{c}_1, \ldots, \tilde{c}_s)^{\mathrm{T}}$, $\boldsymbol{b} = (b_1, \ldots, b_s)^{\mathrm{T}}$ and $\boldsymbol{c} = (c_1, \ldots, c_s)^{\mathrm{T}}$ are s-dimensional vectors of real coefficients. In this work we employ the IMEX-RK scheme H-LDIRK3(2,2,2) defined by

$$\mathcal{A}_{\text{ERK}} = \begin{array}{c|cc} 0 & 0 & 0 \\ 1 & 1 & 0 \\ \hline & 1/2 & 1/2 \end{array}, \qquad \mathcal{A}_{\text{DIRK}} = \begin{array}{c|cc} \gamma & \gamma & 0 \\ 1-\gamma & 1-2\gamma & \gamma \\ \hline & 1/2 & 1/2 \end{array}, \quad \gamma = \frac{3+\sqrt{3}}{6}$$

(see [6,8]). Both the explicit and diagonally implicit parts define third-order schemes [8]. The particular value of γ guarantees that the implicit part is a third-order DIRK scheme with the best dampening properties, see [21] for details.

Now with the aim of applying a particioned Runge-Kutta scheme, consisting in the application of the explicit part to the first block of equations and the implicit part to the second and third blocks, if both Butcher arrays satisfy $\tilde{\boldsymbol{b}} = \boldsymbol{b}$ (as in the case of H-LDIRK3(2,2,2)), then the step from t^n to $t^{n+1} = t^n + \Delta t$ of the linear implicit IMEX-RK scheme is given by the following algorithm.

Algorithm 3.1 (Linearly implicit IMEX-RK (LI-IMEX-RK) scheme)**.**

Input: approximate solution vector $\boldsymbol{u}^n$ and $\boldsymbol{v}^n$ for $t = t^n$
do $i = 1, \ldots, s$

compute the stage values:

$$\boldsymbol{u}^{*(i)} \leftarrow \boldsymbol{u}^n + \Delta t \sum_{j=1}^{i-1} \tilde{a}_{ij} K_j^{\boldsymbol{u}}, \quad \hat{\boldsymbol{u}}^{(i)} \leftarrow \boldsymbol{u}^n + \Delta t \sum_{j=1}^{i-1} a_{ij} K_j^{\boldsymbol{u}}, \quad \hat{\boldsymbol{v}}^{(i)} \leftarrow \boldsymbol{v}^n + \Delta t \sum_{j=1}^{i-1} a_{ij} K_j^{\boldsymbol{v}}$$

compute

$$K_i^{\boldsymbol{v}} \leftarrow -\frac{\varepsilon}{q_{\text{react}}} \frac{\hat{\boldsymbol{v}}^{(i)} \zeta(\boldsymbol{u}^{*(i)})}{1 + (\varepsilon / q_{\text{react}}) \Delta t a_{ij} \zeta(\boldsymbol{u}^{*(i)})} \tag{3.3}$$

solve for $K_i^{\boldsymbol{u}}$ the linear system

$$K_i^{\boldsymbol{u}} = \mathcal{C}\left(\boldsymbol{u}^{*(i)}\right) + \left(\mathcal{D}(\boldsymbol{u}^{*(i)}) - \mathcal{A}\right)\left(\hat{\boldsymbol{u}}^{(i)} + \Delta t a_{ii} K_i^{\boldsymbol{u}}\right) - \left(\hat{\boldsymbol{v}}^{(i)} + \Delta t a_{ii} K_i^{\boldsymbol{v}}\right) \zeta(\boldsymbol{u}^{*(i)})$$

enddo

$$\boldsymbol{u}^{n+1} \leftarrow \boldsymbol{u}^n + \Delta t \sum_{j=1}^{s} b_j K_j^{\boldsymbol{u}}, \qquad \boldsymbol{v}^{n+1} \leftarrow \boldsymbol{v}^n + \Delta t \sum_{j=1}^{s} b_j K_j^{\boldsymbol{v}}$$

Output: approximate solution vectors $\boldsymbol{u}^{n+1}$ and $\boldsymbol{v}^{n+1}$ for $t = t^{n+1} = t^n + \Delta t$.

Observe that $K_i^{\boldsymbol{v}}$ in (3.3) can be computed by evaluating the right-hand in direct form whereas the linear equation for $K_i^{\boldsymbol{u}}$ is solved by using standard and efficient block tridiagonal solvers.

3.3. Linearly implicit IMEX-RK method with Strang-type splitting

An alternative numerical scheme to approximate solutions of (1.1), (2.3) consists in applying a splitting technique, for this, first we consider the ODE system that arises when heat transport and diffusion terms are switched off,

$$\frac{\mathrm{d}\boldsymbol{u}}{\mathrm{d}t} = \boldsymbol{v}\zeta(\boldsymbol{u}), \qquad \frac{\mathrm{d}\boldsymbol{v}}{\mathrm{d}t} = -\frac{\varepsilon}{q_{\text{react}}}\boldsymbol{v}\zeta(\boldsymbol{u}). \tag{3.4}$$

We discretize (3.4) utilizing a time-implicit discretization for $\boldsymbol{v}$ and an explicit one for $\boldsymbol{u}$, i.e.,

$$\boldsymbol{u}^{n+1} = \boldsymbol{u}^{n} + \Delta t\zeta(\boldsymbol{u}^{n})\boldsymbol{v}^{n+1}, \qquad \boldsymbol{v}^{n+1} = \frac{\boldsymbol{v}^{n}}{1+\Delta t(\varepsilon/q_{\text{react}})\zeta(\boldsymbol{u}^{n})}. \tag{3.5}$$

In order to compute (3.5) in each iteration step, we first compute the value of $\boldsymbol{v}^{n+1}$, then this value is used to compute $\boldsymbol{u}^{n+1}$. Now, we define $\psi_{\Delta t} := \mathbb{R}^{M^2}\times\mathbb{R}^{M^2} \to \mathbb{R}^{M^2}\times\mathbb{R}^{M^2}$ as the solution obtained in (3.5) in the way

$$\psi_{\Delta t}(\boldsymbol{u}^{n},\boldsymbol{v}^{n}) = (\boldsymbol{u}^{n+1},\boldsymbol{v}^{n+1}).$$

Next, we solve the system of ordinary differential equations

$$\frac{\mathrm{d}\boldsymbol{u}}{\mathrm{d}t} = \mathcal{C}(\boldsymbol{u}) + \mathcal{D}(\boldsymbol{u})\boldsymbol{u} - \mathcal{A}\boldsymbol{u}, \tag{3.6}$$

then we define $\varphi_{\Delta t} := \mathbb{R}^{M^2}\times\mathbb{R}^{M^2} \to \mathbb{R}^{M^2}\times\mathbb{R}^{M^2}$ by $\varphi_{\Delta t}(\boldsymbol{u}^{n},\boldsymbol{v}^{n}) = (\boldsymbol{u}^{n+1},\boldsymbol{v}^{n})$, where $\boldsymbol{u}^{n+1}$ is the approximation of (3.6) by using Algorithm 3.1. Finally, the Strang splitting method [29] to solve (3.1) is formulated as

$$(\boldsymbol{u}^{n+1},\boldsymbol{v}^{n+1}) = \psi_{\Delta t/2}\circ\varphi_{\Delta t}\circ\psi_{\Delta t/2}(\boldsymbol{u}^{n},\boldsymbol{v}^{n}). \tag{3.7}$$

4. Numerical results

In the following examples, we solve (3.1) numerically for $0 \le t \le T$ and $(x,y) \in \Omega := (0,L)^2$, under various choices of the initial datum u_0 and v_0. Numerical results are obtained by the linearly implicit IMEX scheme denoted by LIMEX (see Algorithm 3.1), and the Strang-type splitting scheme (3.7) called S-LIMEX. We consider a Cartesian uniform mesh grid of M^2 points and $\Delta x = \Delta y = L/M$. We denote by Δt the time step used to advance the numerical solution from $t = t^n$ to $t^{n+1} = t^n + \Delta t$. For each iteration Δt is determined by the following usual formula (CFL condition)

$$\frac{\Delta t}{\Delta x}\|\boldsymbol{w}\|_\infty = \frac{1}{2}\mathrm{C}_{\text{cfl}}.$$

In all numerical test we have used $C_{\text{cfl}} = 0.12$.

4.1. Example 1: Propagation of a wildfire with constant initial distribution of fuel

In this example we compare the approximations obtained by both schemes, S-LIMEX and LIMEX, for different discretizations and simulated times. We consider first a configuration that allows us to compare our results with those of [2], that is, we solve (1.1) on the domain Ω with $L = 50$ in dimensionless variables, which corresponds to a square of side length $50l_0 = 14.99\,\mathrm{m}$. We choose the dimensionless wind vector $\boldsymbol{w} = (w_1, w_2) = (300, 300)$, which blows in north-east direction at physical speed $\|\boldsymbol{v}\| = (l_0/t_0)\|\boldsymbol{w}\| \approx 0.0142\,\mathrm{m\,s^{-1}}$. (Much larger values seem more realistic.) The initial conditions for the non-dimensional temperature and the fuel are

$$u_0(x,y) = 31\chi_{[4,12]^2}(x,y), \qquad v_0(x,y) = 0.6\chi_{\Omega}(x,y).$$

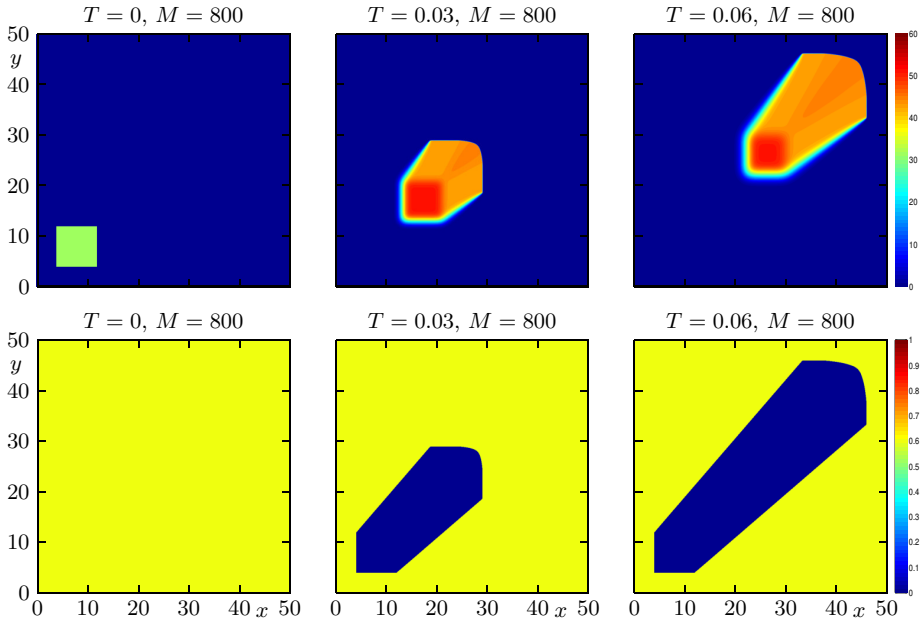

Figure 1. Example 1: Numerical approximation with S-LIMEX for $\Delta x = \Delta y = 50/800$.

	LIMEX			S-LIMEX		
M	$e_M(u)$	$e_M(v)$	cpu[s]	$e_M(u)$	$e_M(v)$	cpu[s]
	$T = 0.03$					
50	2.32	2.1e-2	0.7	1.74	1.5e-2	0.3
100	1.22	1.8e-2	6.3	1.11	9.6e-3	3.5
200	0.96	1.1e-2	19.1	0.83	8.1e-3	18.8
400	0.59	6.3e-3	133.6	0.59	6.6e-3	162.0
800	0.27	3.3e-3	1012.6	0.32	3.8e-3	1405.0
	$T = 0.06$					
50	4.01	7.5e-2	3.2	2.99	3.8e-2	1.2
100	3.12	4.2e-2	13.3	2.54	3.3e-2	7.7
200	2.38	3.6e-2	38.6	2.05	2.8e-2	36.9
400	1.51	2.1e-2	266.6	1.51	2.2e-2	324.7
800	0.72	1.1e-2	2004.7	0.87	1.3e-2	2737.4

Table 1. Example 1: approximate L^1 errors $e_M(u)$, $e_M(v)$ and CPU time.

We display the numerical approximation obtained with both schemes in Figs. 1 and 2, with $\Delta x = \Delta y = 50/400$ at simulated times $T = 0.03$ and $T = 0.06$, which represent 4.5 and 9 minutes approximately . The dynamics of the propagation of wildfire is comparable with those results of [2]. In Figure 3 (left) we display the evolution of the non-dimensional temperature in a short time on the diagonal $y = x$ of the domain Ω, numerical approximation was computed with S-LIMEX scheme with $\Delta x = \Delta y = 50/800$, corresponding to time step $\Delta t = 7.8125 \times 10^{-6}$. The highest temperature reached during the initial steps does not exceed the maximum $U_{\max}$ for the given parameters and initial conditions chosen, also we observe the formation of a fire front travelling in a direction parallel to the vector $\boldsymbol{w}$. In Figure 3 (right) we compare the numerical approximation for both numerical schemes with respect to the reference solution for two discretization levels with $\Delta x = \Delta y = 50/M$ for $M = 100$ and $M = 200$, corresponding to $\Delta t = 6.25 \times 10^{-5}$ and$\Delta t = 3.125 \times 10^{-5}$, respectively, where we have represented the non-dimensional temperature at simulated time $T = 0.06$ on the diagonal $y = x$. We observe that the numerical approximations are qualitatively equivalent. In Table 1 we compute the approximate L^1-errors $e_M(u)$ and $e_M(v)$ for both numerical schemes computed with different discretizations $\Delta x = \Delta y = 50/M$ and $M = 50$, 100, 200, 400, and 800, with respect to a reference solution computed with S-LIMEX scheme with $M = 3200$. For these cases, we employ $\Delta t = 1.25 \times 10^{-4}$

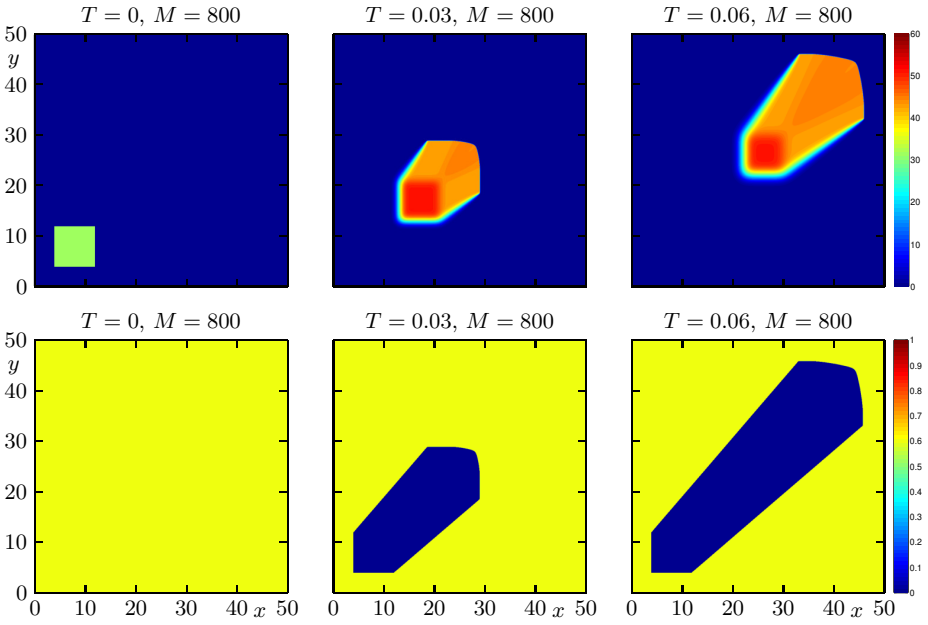

Figure 2. Example 1: Numerical approximation with LIMEX for $\Delta x = \Delta y = 50/800$.

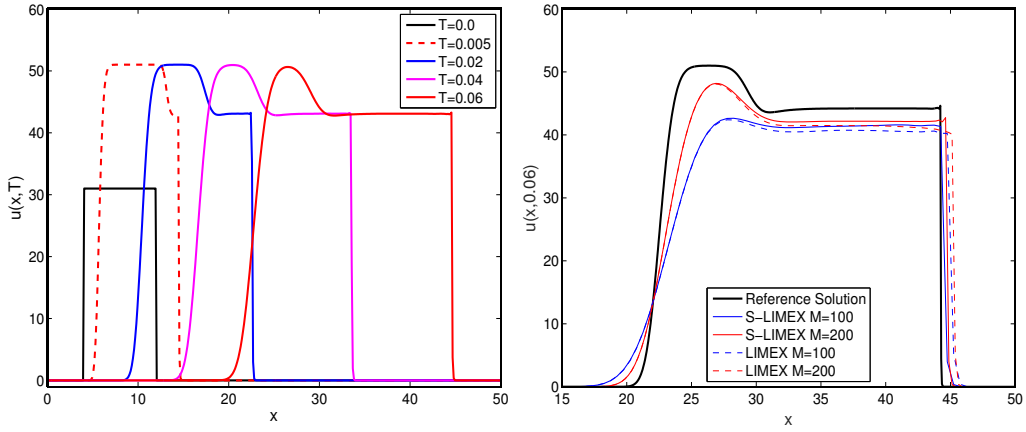

Figure 3. Example 1: 1-D Projection over the line $y = x$ (Left) evolution of the non-dimensional temperature in a short time (Right) Comparison numerical approximation with LIMEX and S-LIMEX respect to Reference solution, with $M = 200$ and $M = 400$ at $T = 0.16$.

for the coarse mesh and $\Delta t = 7.8125 \times 10^{-6}$ for the finer mesh. We observe that for the coarse mesh, the S-LIMEX scheme is more accurate than the LIMEX scheme, however for a finer mesh, LIMEX is more accurate and faster than the S-LIMEX scheme.

4.2. Example 2: Propagation of a wildfire with distribution of fuel determined by two areas with different fuel densities

In this example we describe the dynamics of the wildfire when it enters a region with different fuel density. We consider $\Omega := (0, 200) \times (0, 200)$, $\varepsilon = 0.035$, $u_{\text{pc}} = 20$ and $\boldsymbol{w} = (300, 300)$. First, we employ the initial conditions

$$u_0(x, y) = 21\chi_{[9,21]^2}(x, y), \quad v_0(x, y) = \begin{cases} 0.45 + \delta(x, y) & \text{for } x \leq 100, \\ 0.70 + \delta(x, y) & \text{for } x > 100, \end{cases} \tag{4.1}$$

where δ is a function that is piecewise constant and constant on each cell of the computational grid, and takes random values with $|\delta(x, y)| \leq 0.025$. Notice that the initial density of fuel is higher for $x > 100$

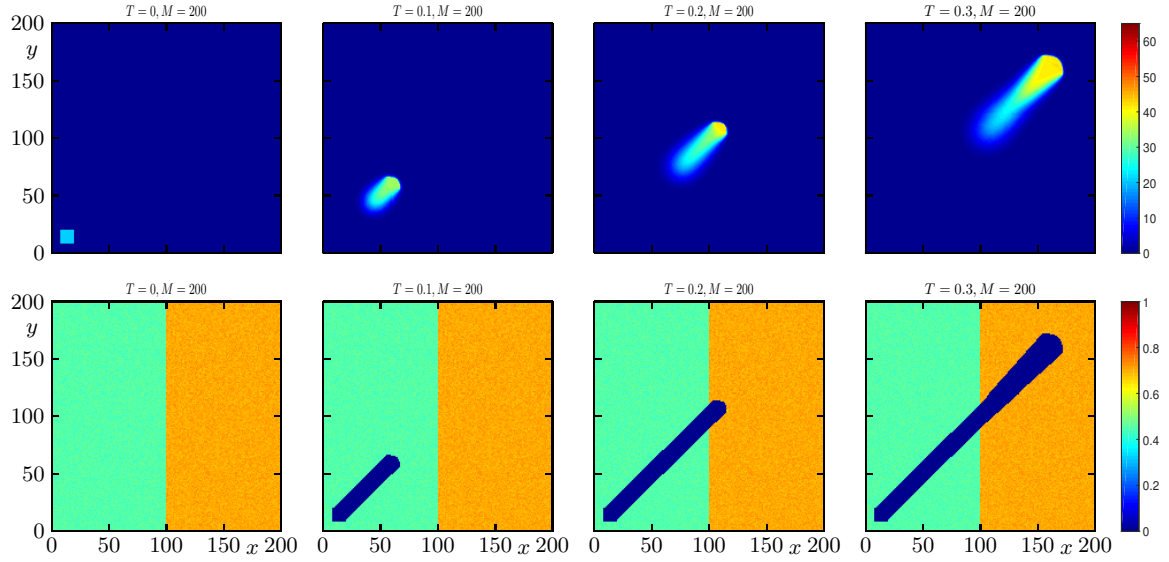

Figure 4. Example 2: Simulation when the wildfire enters a region with higher fuel density.

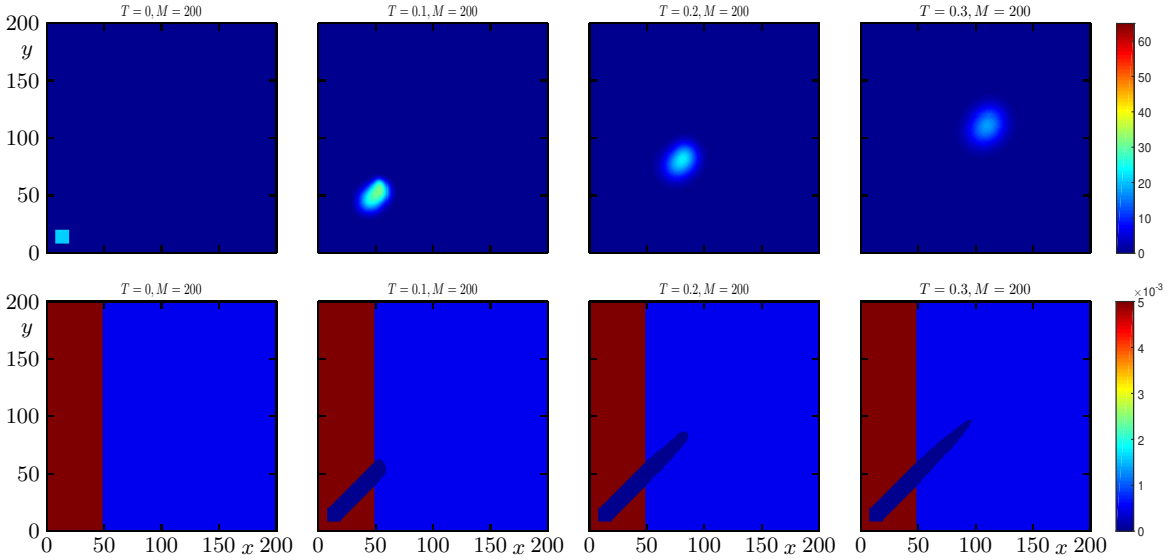

Figure 5. Example 2: Simulation when the wildfire enters a region with a very low fuel density.

than for $x < 100$. In Figure 4 we display the numerical solution at four simulated times, namely the initial condition at $T = 0$ and the solution at $T = 0.1$, $T = 0.2$, and $T = 0.3$. We observe that when the wildfire enters a region with higher fuel density, the non-dimensional temperature increases and the width of the fire in the main direction of propagation is higher than in the less dense area, and this width increases with time and the fire *opens*.

Now we employ the same initial condition for temperature, but to detect where the fire is extinguished due to low availability, we will consider only the left half of the same less dense area and to its right a test area with a very low and close to zero fuel density. To this end we impose

$$v_0(x,y) = \begin{cases} 0.45 & \text{for } x \leq 50, \\ 5 \times 10^{-4} & \text{for } x > 50. \end{cases}$$

In Figure 5 we display the numerical solution at four simulated times, namely the initial condition at $T = 0$ and the solution at $T = 0.1$, $T = 0.2$, and $T = 0.3$. We observe that when the wildfire enters a

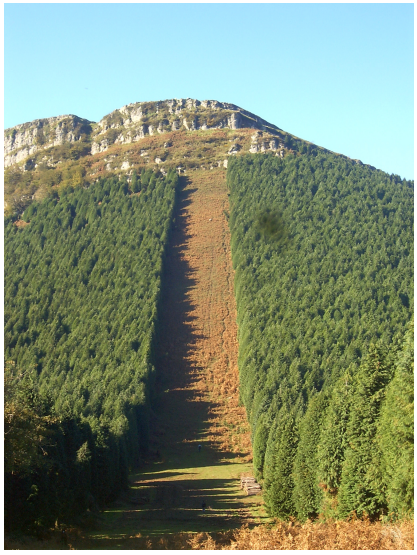

Figure 6. An example of a firebreak (see https://es.wikipedia.org/wiki/Archivo:Eretza_2.jpg).

region with a very low fuel density, the fire focus width decreases with time and tends to disappear since the temperature of the focus always remains below u_{pc} when it has already traveled more than 100 (unit lengths). This behavior allows one to identify the horizontal length after which the fire is extinguished (at the given wind speed).

The numerical resuts in Figures 4 and 5 were computed with S-LIMEX scheme with $\Delta x = \Delta y = 200/M$ and $M = 200$, corresponding a time step $\Delta t = 1.25 \times 10^{-4}$.

4.3. Example 3: Effect of a firebreak in the propagation of a wildfire

In the prevention and control of forest fires, the role played by the implementation or construction of firebreaks (see Figure 6) is very important, whose role is to mitigate the effect of a fire or ideally prevent the spread of fire, this is usually done through the construction of a space rectangular whose objective is to separate two zones so as to be able to protect a certain zone, which could be a forest with a large amount of fuel from which you can obtain wood for commercial uses, a native forest that you want to take care of, or a set of households. To implement this fire control strategy using firebreaks, it is essential to study the effects that produce different values for the length corresponding to the width of said area with a fuel density of very low or equal to zero.

The above motivates this third example where we would like to observe the effect of a firebreak in the propagation of a wildfire separaing two areas with different fuel distribution. We consider parameters as in Example 2 with u_0 as in (4.1) and initial distribution of fuel given by

$$v_0(x,y) = \begin{cases} 0.45 + \delta(x,y) & \text{for } x \leq 100 - l, \\ 0.7 + \delta(x,y) & \text{for } x > 100, \end{cases}$$

where again where δ is a function that is piecewise constant and constant on each cell of the computational grid, and takes random values with $|\delta(x,y)| \leq 0.025$, and where $l > 0$ is the width of strip corresponding to a firebreak sepataring the two areas. Here we will consider two cases for the value l, the first when $l = 25$ and the second when $l = 50$ units of length.

In the case $l = 25$, we display in Figure 7 the dynamics of propagation of the wildfire at four different simulated times. We observe that when the wildfire front crosses the firebreak region, the magnitude of the non-dimensional temperature decreases, however the wildfire does not extinguish and crosses to the area with high fuel density. Its temperature increase and the fire focus becomes wider. In Table 2 we compute the total amount of fuel in the denser area for different widths of the

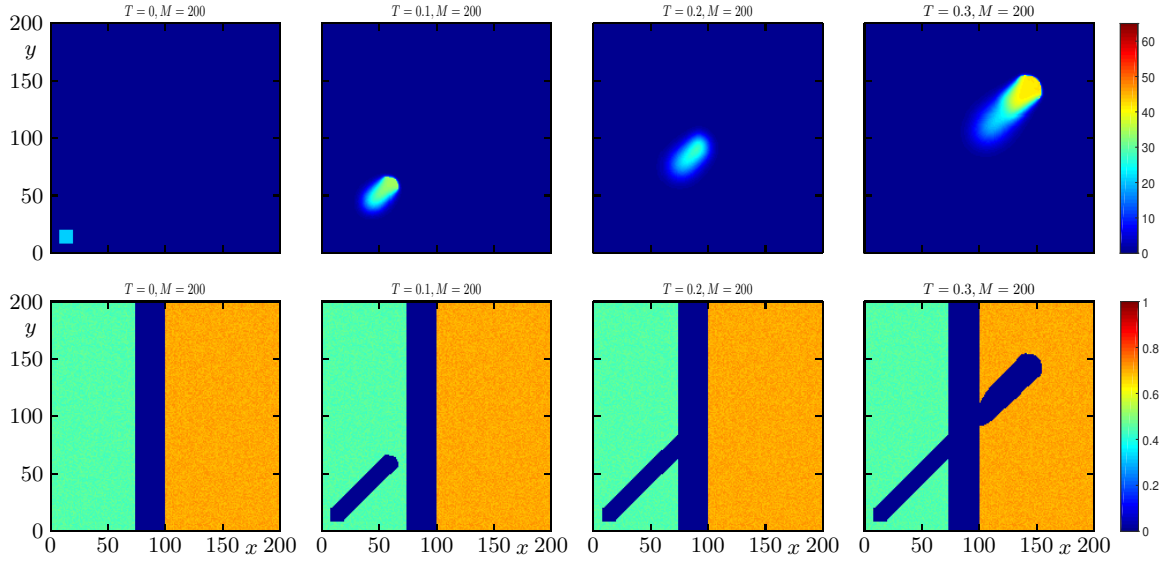

Figure 7. Example 3: Propagation of fire across a firebreak of insufficient width.

firebreak. We observe that amount of fuel burnt for $l = 25$ is smaller than for $l = 0$, see also Figure 4 corresponding to the first part of Example 2.

Time	$l = 0$	$l = 25$	$l = 50$
$T = 0.1$	14000.93	14000.93	14000.93
$T = 0.2$	13826.65	10815.72	14000.93
$T = 0.3$	12699.81	12956.04	14000.93

Table 2. Values for the proportion of fuel in the densest area at different times.

On the other hand, when $l = 50$, we can see in the Figure 8 that the wildfire is extinguished and does not cross from the area with the lowest fuel density to the area with the highest density.

The obtained in these two scenarios agrees with with what was obtained in the second part of the previous Example, since there it can be seen that the temperature is below the value of $u_{\text{pc}} = 20$ and remains so over time for a value of x less than 100, which suggests the width of the firebreak should be approximately 50 units of length. The numerical results of Figure 9 was computed with S-LIMEX scheme with $\Delta x = \Delta y = 200/M$ and $M = 200$, corresponding a time step $\Delta t = 1.25 \times 10^{-4}$.

4.4. Example 4: Propagation of a wildfire with randomized initial distribution of fuel and a slight change of direction in the wind

For a macroscopic scale, the wind direction is generally variable, but when considering on a smaller scale a fixed region that is of interest in the context of forest fires it is observed that said direction can be considered constant or at most with a slight variation of it. In this configuration we consider Ω with $L = 200$ in dimensionless variables, which corresponds to a square of side length $200 l_0 = 59.96\,\text{m}$ with a randomized initial distribution of fuel in the whole domain. We choose initially the dimensionless wind vector $\boldsymbol{w} = (300, 300)$ and we change the wind direction at time $T = 0.085$, which represents approximately 14 minutes, to $\boldsymbol{w}^* = (50, 400)$. We would like observe the dynamics in the wildfire at simulated time $T = 0.15$. The initial values for the non-dimensional temperature and the fuel distribution are

$$u_0(x, y) = 38\chi_{[2,14]^2}(x, y), \qquad v_0(x, y) = 0.5 + \delta(x, y)$$

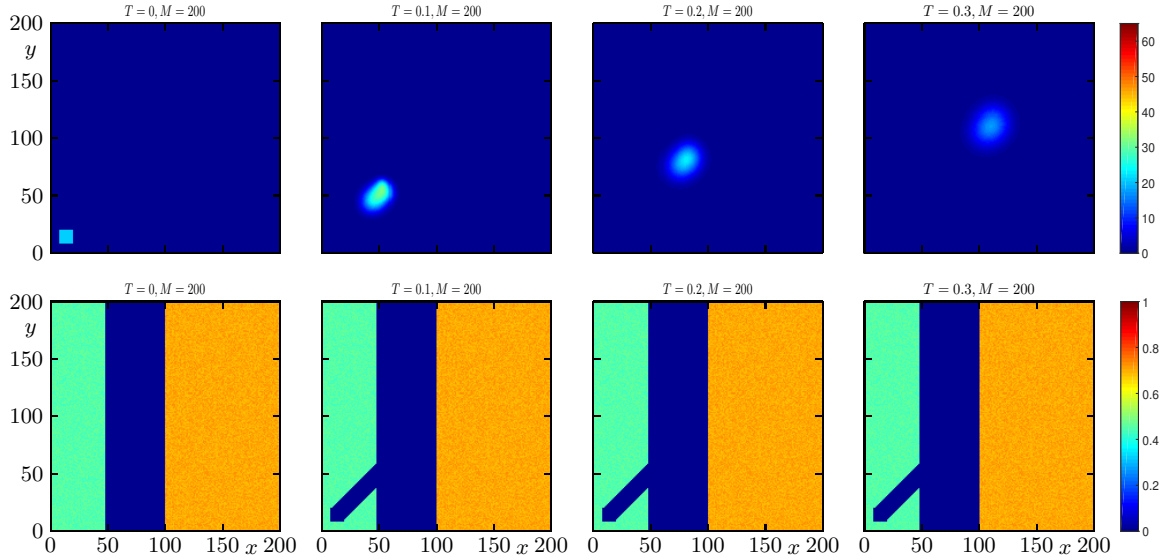

Figure 8. Example 3: Extinction of fire by a sufficiently wide firebreak.

where δ is a function that is piecewise constant and constant on each cell of the computational grid, and takes random values with $|\delta(x, y)| \leq 0.4$.

In Figure 9 we can observe the effect of the change of the wind in the wildfire. From the initial time with w as direction in the wind until before the simulated time $T = 0.085$ it can be seen that the strip corresponding to the burned fuel has a certain constant thickness and when the direction of the wind changes to w^* we observe an increase in the thickness of the strip of the burned area is appreciated. The numerical resultsin Figure 9 were obtained by the S-LIMEX scheme with $\Delta x = \Delta y = 100/M$ and $M = 400$, corresponding a time step $\Delta t = 6.25 \times 10^{-5}$.

5. Conclusions

In the present work for the model defined by (2.1) and (2.2) we have implemented two numerical methods that allow studying this system of equations. The first method is a linearly implicit IMEX-RK scheme and is described in Section 3.2, the second Linearly method implicit IMEX-RK method with Strang-type splitting is described in Section 3.3. Both numerical methods allow us to study the evolution of the temperature and fuel variables over time based on certain initial conditions. In the first instance, we worked with both methods in order to study the evolution of numerical simulations such as those observed in Figures 1 and 2, where considering a certain set of parameters it is observed that the fire focus tends to move through the domain according to the direction of the wind speed and that given a certain constant fuel density, this focus increases as time passes. Both methods are compared according to the projection of the fire front on the diagonal of the domain, which is shown in Figure 3.

On the other hand, to show the application of the second numerical method from a practical point of view we have designed a strategy, knowing that when the availability of fuel is very low then the wildfire tends to be extinguished by the effect of diffusion and convection so as to detect the horizontal distance that the fire front travels before it is completely extinguished, which can be seen in Figure 5. This then allows us to build a firebreak in order to mitigate the effect of the fire or totally prevent its passage towards a certain area which must be protected and thus avoid what is seen in Figure 4. Then considering the ideal length obtained for the width of said firebreak we proceed to compare two situations, one in which the length is less than the ideal and whose effect is partial in the sense that the fire does transfer to the side that is interested in protecting, only achieving less fuel consumption (Figure 7) than in the case when firebreak is absent. On the other hand, when considering the ideal length we can see that this new firebreak effectively achieves the function of preventing the fire front

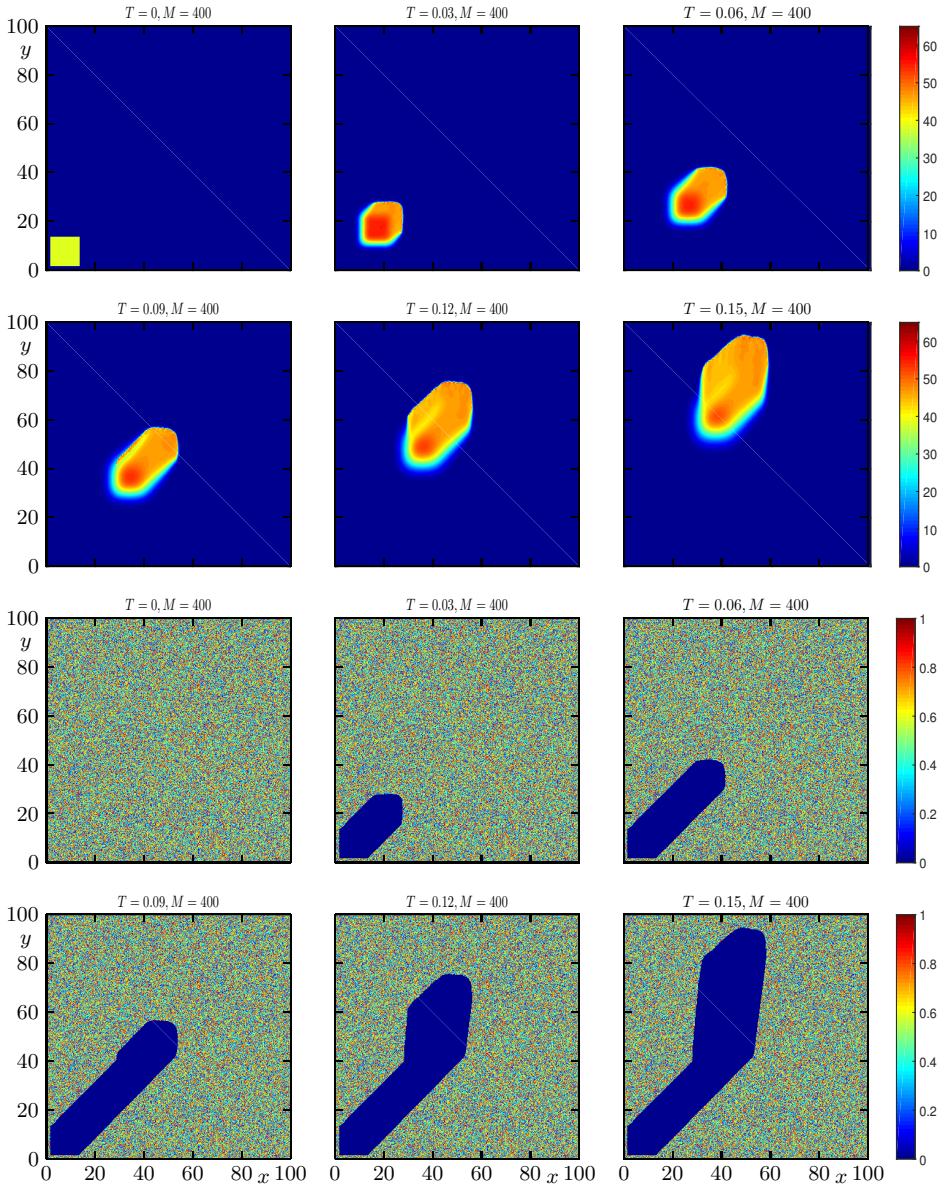

Figure 9. Example 4: Evolution of the non-dimensional temperature and proportion of fuel in space under a change of the wind direction.

from passing into the area that it is interested in protecting (Figure 8). We have also studied what happens when a slight change in the direction of the wind occurs in a certain domain, which has the effect of considerably widening the width of the focus of the fire as shown in Figure 9.

The authors' interest in the numerical solution of the wildfire propagation model (1.1) is partially motivated by experience with IMEX methods, and in particular the gain of efficiency achieved with these methods, for related applicative nonlinear convection-diffusion problems [6,7,10–13]. While the results presented herein are basically encouraging and reconfirm that the model can in principle be used for the prediction of wildfire propagation and its mitigation through cutting firebreaks of sufficient width, further work is required to establish IMEX methods as a really competitive tool for wildfire simulation. One aspect is related to the discretization of the reaction terms. The present version of the Strang splitting method is still based on using a single time step for the whole computational domain. It could probably be made more efficient by local time stepping so that time-consuming small time steps are employed only where it is necessary. On the other hand, several model ingredients still need to be incorporated, including topography of the terrain (as expressed by the function $h(\boldsymbol{x})$ that

describes spatial heterogeneity but which has been chosen constant here; see Section 2.2), as well as radiation, moisture content and pyrolisis via a multivalued enthalpy function as in [18,19]).

Acknowledgments

RB is supported by CRHIAM, project ANID/FONDAP/15130015 and Fondecyt project 1170473. DI acknowledges CONICYT scholarship CONICYT-PCHA/Doctorado Nacional/2014-21140362. PM is supported by Spanish MINECO project MTM2017-83942-P and Conicyt (Chile), project PAI-MEC, folio 80150006. LMV is supported by Fondecyt project 1181511. RB, DI and LMV are also supported by CONICYT/PIA/Concurso Apoyo a Centros Científicos y Tecnológicos de Excelencia con Financiamiento Basal AFB170001, and by the INRIA Associated Team "Efficient numerical schemes for non-local transport phenomena" (NOLOCO; 2018–2020).

References

1. Ascher, U.; Ruuth, S.; Spiteri, J. Implicit-explicit Runge-Kutta methods for time dependent partial differential equations. *Appl. Numer. Math.* **1997**, *25*, 151–167.
2. Asensio, M.I.; Ferragut, L. On a wildland fire model with radiation. *Int. J. Numer. Meth. Engrg.* **2002**, *54*, 137–157.
3. Barovik, D.; Taranchuk, V. Mathematical modelling of running crown forest fires. *Math. Model. Anal.* **2010**, *15*, 161–174.
4. Barrow, G.M. *Physical Chemistry*; McGraw-Hill: New York, 1966.
5. Bebernes, J.; Eberly, D. *Mathematical Problems from Combustion Theory*; Springer: New York, 1989.
6. Boscarino, S.; Bürger, R.; Mulet, P.; Russo, G.; Villada, L.M. Linearly implicit IMEX Runge-Kutta methods for a class of degenerate convection-diffusion problems. *SIAM J. Sci. Comput.* **2015**, *37*, B305–B331.
7. Boscarino, S.; Bürger, R.; Mulet, P.; Russo, G.; Villada, L.M. On linearly implicit IMEX Runge-Kutta Methods for degenerate convection-diffusion problems modelling polydisperse sedimentation. *Bull. Braz. Math. Soc. (N. S.)* **2016**, *47*, 171–185.
8. Boscarino, S.; Filbet, F.; Russo, G. High order semi-implicit schemes for time dependent partial differential equations. *J. Sci. Comput.* **2016**, *68*, 975–1001.
9. Boscarino, S.; LeFloch, P.G.; Russo, G. High order asymptotic-preserving methods for fully nonlinear relaxation problems. *SIAM J. Sci. Comput.* **2014**, *36*, A377–A395.
10. Bürger, R.; Chowell, G.; Gavilán, E.; Mulet, P.; Villada, L.M. Numerical solution of a spatio-temporal gender-structured model for hantavirus infection in rodents. *Math. Biosci. Eng.* **2018**, *15*, 95–123.
11. Bürger, R.; Chowell, G.; Gavilán, E.; Mulet, P.; Villada, L.M. Numerical solution of a spatio-temporal predator-prey model with infected prey. *Math. Biosci. Eng.* **2019**, *16*, 438–473.
12. Bürger, R.; Inzunza, D.; Mulet, P.; Villada, L.M. Implicit-explicit schemes for nonlinear nonlocal equations with a gradient flow structure in one space dimension. *Numer. Methods Partial Differential Equations* **2019**, *35*, 1008–1034.
13. Bürger, R.; Inzunza, D.; Mulet, P.; Villada, L.M. Implicit-explicit methods for a class of nonlinear nonlocal gradient flow equations modelling collective behaviour. *Appl. Numer. Math.* **2019**, *144*, 234–252.
14. Bürger, R.; Mulet, P.; Villada, L.M. Regularized nonlinear solvers for IMEX methods applied to diffusively corrected multi-species kinematic flow models. *SIAM J. Sci. Comput.* **2013**, *35*, B751–B777.
15. Butcher, J.C. *Numerical Methods for Ordinary Differential Equations*, second ed. Wiley: Chichester, UK, 2008.
16. Donat, R.; Guerrero, F.; Mulet, P. Implicit-explicit methods for models for vertical equilibrium multiphase flow. *Comput. Math. Appl.* **2014**, *68*, 363–383.
17. Eberle, S.; Freeden, W.; Matthes, U. Forest fire spreading. In *Handbook of Geomathematics*, second ed.; Freeden, W., Nashed, M.Z., Sonar, T., Eds.; Springer-Verlag: Berlin, Germany, 2015; pp. 1349–1385.
18. Ferragut, L.; Asensio, M.I.; Monedero, S. Modelling radiation and moisture content in fire spread. *Commun. Numer. Meth. Engrg.* **2007**, *23*, 819–833.
19. Ferragut, L.; Asensio, M.I.; Monedero, S. A numerical method for solving convection-reaction-diffusion multivalued equations in fire spread modelling. *Adv. Engrg. Software* **2007**, *38*, 366–371.

20. Frank-Kamenetskii, D.A. *Diffusion and Heat Transfer in Chemical Kinetics*. Princeton University Press: Princeton, NJ, USA, 1955.
21. Hairer, E.; Nørsett, S.P.; Wanner, G. *Solving Ordinary Differential Equations. I. Non-stiff Problems*, Springer Series in Computational Mathematics, vol 8. Springer: Berlin, 1993.
22. Manual of good practices in forest fires prevention. *Generalitat Valenciana.*
23. Ortega, M. Manual medidas prediales de protección contra incendios forestales. *Documento de trabajo 451, Corporación Nacional Forestal, Chile*, **2006**.
24. Pareschi, L.; Russo, G. Implicit-Explicit Runge-Kutta schemes and applications to hyperbolic systems with relaxation. *J. Sci. Comput.* **2005**, *25*, 129–155.
25. Pastor, E.; Zárate, L.; Planas, E.; Arnaldos, J. Mathematical models and calculation systems for the study of wildland fire behaviour. *Progr. Energy Combust. Sci.* **2003**, *29*, 139–153.
26. Prieto, D.; Asension, M.I.; Ferragut, L.; Cascón, J.M.; Morillo, A. A GIS-based fire spread simulator integrating a simplified physical wildland fire model and a wind field model. *Int. J. Geograph. Inf. Sci.* **2017**, *31*, 2142–2163.
27. San Martín, D.; Torres, C.E. Ngen-Kütral: Toward an open source framework for Chilean wildfire spreading. 37th International Conference of the Chilean Computer Science Society (SCCC). SCCC: Santiago, Chile, 2018; pp. 1–8.
28. San Martín, D.; Torres, C.E. Exploring a spectral numerical algorithm for solving a wildfire mathematical model. 38th International Conference of the Chilean Computer Science Society (SCCC). SCCC: Concepción, Chile, 2019; pp. 1–7.
29. Strang, G. On the construction and comparison of difference schemes. *SIAM J. Numer. Anal.* **1968**, *5*, 506–517.

Centro de Investigación en Ingeniería Matemática (CI^{2}MA)

PRE-PUBLICACIONES 2019 - 2020

2019-44 Nestor Sánchez, Tonatiuh Sanchez-Vizuet, Manuel Solano: *A priori and a posteriori error analysis of an unfitted HDG method for semi-linear elliptic problems*

2019-45 Mauricio Munar, Filander A. Sequeira: *A posteriori error analysis of a mixed virtual element method for a nonlinear Brinkman model of porous media flow*

2019-46 Raimund Bürger, Stefan Diehl, María Carmen Martí, Yolanda Vásquez: *On dynamic models of flotation with sedimentation*

2019-47 Raimund Bürger, Sarvesh Kumar, David Mora, Ricardo Ruiz-Baier, Nitesh Verma: *Virtual element methods for the three-field formulation of time-dependent linear poroelasticity*

2019-48 Gabriel R. Barrenechea, Fabrice Jaillet, Diego Paredes, Frederic Valentin: *The multiscale hybrid mixed method in general polygonal meshes*

2020-01 Sergio Caucao, Gabriel N. Gatica, Ricardo Oyarzúa, Nestor Sánchez: *A fully-mixed formulation for the steady double-diffusive convection system based upon Brinkman–Forchheimer equations*

2020-02 Gonzalo A. Benavides, Leonardo E. Figueroa: *Orthogonal polynomial projection error in Dunkl-Sobolev norms in the ball*

2020-03 Rodolfo Araya, Abner Poza, Frederic Valentin: *An adaptative multiscale hybrid-mixed method for the Oseen equations*

2020-04 Carlos Parés, David Zorío: *Lax Wendroff approximate Taylor methods with fast and optimized weighted essentially non-oscillatory reconstructions*

2020-05 Julio Aracena, Lilian Salinas: *Finding the fixed points of a Boolean network from a positive feedback vertex set*

2020-06 Tomás Barrios, Rommel Bustinza, Camila Campos: *A note on a posteriori error estimates for dual mixed methods*

2020-07 Raimund Bürger, Elvis Gavilán, Daniel Inzunza, Pep Mulet, Luis M. Villada: *Numerical simulation of forest fires by IMEX methods*

Para obtener copias de las Pre-Publicaciones, escribir o llamar a: Director, Centro de Investigación en Ingeniería Matemática, Universidad de Concepción, Casilla 160-C, Concepción, Chile, Tel.: 41-2661324, o bien, visitar la página web del centro: `http://www.ci2ma.udec.cl`







Centro de Investigación en
Ingeniería Matemática (CI²MA)
Universidad de Concepción

Casilla 160-C, Concepción, Chile
Tel.: 56-41-2661324/2661554/2661316
http://www.ci2ma.udec.cl